

Tucker, R.T., et al., 2023, Exceptional age constraint on a fossiliferous sedimentary succession preceding the Cretaceous Thermal Maximum: *Geology*, <https://doi.org/10.1130/G51278.1>

Supplemental Material

Table S1, Bulk rock XRF results

Table S2, Bulk rock XRD results

Figure S1, Classification of volcaniclastics via A) La Maitre-IUGS and B) Peccerillo & Taylor.

Table S3, GPS locations of samples collected in decimal degrees (Map Datum and Map Spheroid in WGS 84)

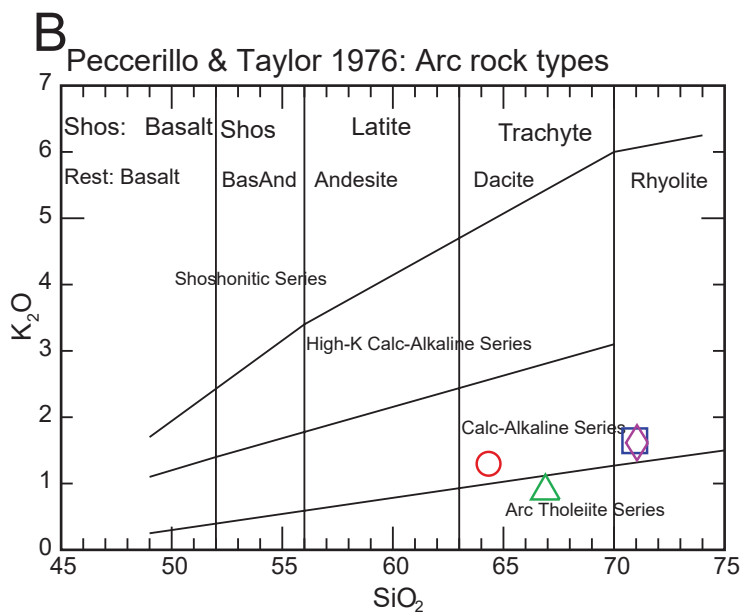
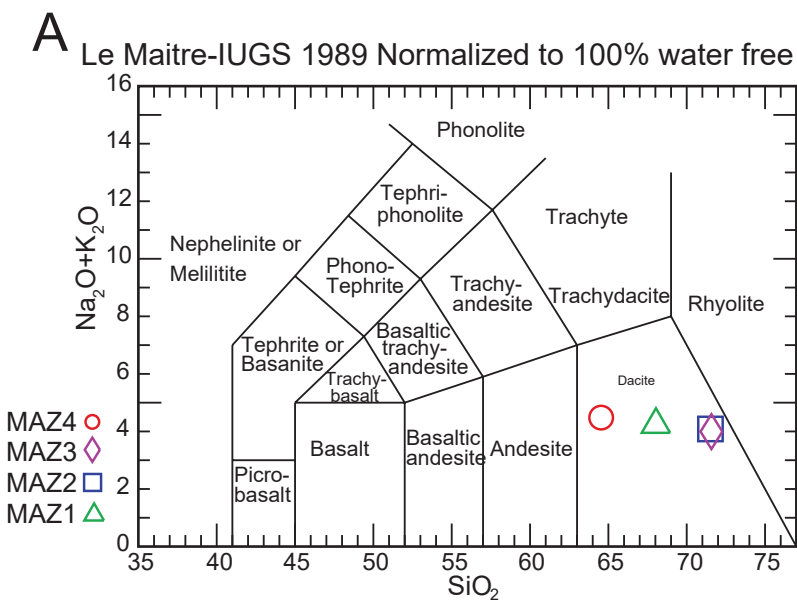
Extended Methods and Results

Cathodoluminescence images of zircon grains collected via scanning electron microscope. LA-ICP-MS spots and labels are shown.

Table S4, CA-TIMS zircon U-Pb isotopic data Data table with Grain Shape

Tables S5–S16, Metadata for LA-ICP-MS U-(Th-)Pb analyses

Table S17, Bayesian algorithm of Keller Table



For classification, we coupled XRD and XRF. Our units fit the definition “volcanic ash fall” by Hong et al. (2019), consisting of 70–80% glass, 20–25% phenocrysts, and minor amorphous clays. Based on XRD results, the presence of quartz crystals and more significant amounts of plagioclase (10–20%) as opposed to orthoclase (0.8–4.5%), coupled with XRF-based IUGS classification of volcanic rocks (Fig. 3A), all four samples classify as dacitic. These dacites are borderline tholeiitic to medium-K calc-alkaline (Peccerillo and Taylor, 1976) (Fig. 3B). In detail, MAZ1 and MAZ4 are slightly more primitive than the remarkably similar MAZ2 and MAZ3 (Fig. 3 C,D). We interpret the moderate levels of an unidentified amorphous fraction (39–53%) coupled with high SiO₂ values as glass instead of meta-Kaolin. Although we can roughly identify these as crystal tuffs due to the age and levels of smectite present (13–20%), we prefer to identify them as tuffaceous bentonites. Each ash bed typically weathers into haystacks with popcorn weathering, jigsaw puzzle clay fractures, and nodular masses (“eggs”). However, with closer examination, we found significant amounts of Mg (mixing of brackish waters), mineral content (anhedral biotite and euhedral zircon), whole-rock abundances of Al, Fe, Mg, K, and quantities of Ti vary inversely with Si, along with variation in internal layering, layer charge, variable clay ratios, and wet color modification; we can infer that with further devitrification MAZ1–4 would be classified as K-bentonites (Huff, 2016).

LA-ICP-MS methods

Zircon grains were separated from rocks using standard crushing, heavy-liquid, and magnetic separation techniques. Only sharply faceted grains were picked and annealed at 900°C for 60 hours in a muffle furnace. Grains were mounted in epoxy and polished until their centers were exposed. One sample (COI-2) has too small grains for mounting and polishing.

Cathodoluminescence (CL) images were obtained from a Hitachi S-3400N-II scanning electron microscope. Laser ablation inductively coupled plasma mass spectrometry (LA-ICPMS) analyses on zircon grains were performed on an iCAP RQ Quadrupole ICP-MS and Teledyne Photon Machines Analyte Excite+ 193 nm excimer laser ablation system with HeEx II Active two-volume ablation cell. In-house analytical protocols, standard materials, and data reduction software were used for the acquisition and calibration of U-Pb dates and a suite of high-field strength elements (HFSE) and rare earth elements (REE). Zircon grains were ablated with a laser spot of 20 μm wide using fluence and pulse rates of 2.5 J/cm² and 10 Hz, respectively, during a 25-second analysis (15-sec gas blank, 10-sec ablation) that excavated a pit \sim 7 μm deep. Ablated material was carried by a 0.25 L/min He gas stream in the inner cell and a 1.25 L/min He gas stream in the outer cell. Dwell times and other instrumental data are given in Table S1, which accompanies the sample data tables. Background count rates for each analyte were obtained before each spot analysis and subtracted from the raw count rate for each analyte. Ablation pits that appear to have intersected glass or mineral inclusions were identified based on Ti, and P. U-Pb dates from these analyses are considered valid if the U-Pb ratios appear to have been unaffected by the inclusions. Analyses that appear contaminated by common Pb were rejected based on mass 204 being above baseline. For concentration calculations, background-subtracted count rates for each analyte were internally normalized to ²⁹Si and calibrated concerning NIST

SRM-610 and -612 glasses as the primary standards. The Ti-in-zircon thermometer calculated the temperature (Watson et al., 2006). Because there are no constraints on the activity of TiO_2 , an average value in crustal rocks of 0.6 was used.

Data were obtained in three experiments in May 2022. For U-Pb and $^{207}\text{Pb}/^{206}\text{Pb}$ dates, instrumental fractionation of the background-subtracted ratios was corrected, and dates were calibrated concerning interspersed measurements of zircon standards and reference materials. The primary standard Plešovice zircon (Sláma et al., 2008) was used to monitor time-dependent instrumental fractionation based on two analyses for every 12 analyses of unknown zircon. A secondary correction to the $^{206}\text{Pb}/^{238}\text{U}$ dates was made based on results from the zircon standards Seiland (531 Ma, Kuiper et al., 2022) and 91500 (1065 Ma, Wiedenbeck et al., 1995), which were treated as unknowns and measured once for every 12 analyses of unknown zircon. These results (Table S3) showed a linear age bias of several percent related to the ^{206}Pb count rate. The secondary correction is thought to mitigate matrix-dependent variations due to contrasting compositions and ablation characteristics between the Plešovice zircon and other standards (and unknowns).

Radiogenic isotope ratio and age error propagation for all analyses include uncertainty contributions from counting statistics and background subtraction. Errors without and with the standard calibration uncertainty are shown in Table S2. This uncertainty is the local standard deviation of the polynomial fit to the interspersed primary standard measurements versus time for the time-dependent, relatively larger U/Pb fractionation factor, and the standard error of the mean of the consistently time-invariant and smaller $^{207}\text{Pb}/^{206}\text{Pb}$ fractionation factor. These uncertainties are given in Table S1. Errors on single analyses without the standard calibration uncertainty are given below. Age interpretations are based on $^{207}\text{Pb}/^{206}\text{Pb}$ dates for analyses with

$^{207}\text{Pb}/^{206}\text{Pb}$ and $^{206}\text{Pb}/^{238}\text{U}$ dates >1500 Ma. Otherwise, interpretations are based on $^{206}\text{Pb}/^{238}\text{U}$ dates. Analyses with discordance, defined as the relative difference between the $^{207}\text{Pb}/^{235}\text{U}$ and $^{206}\text{Pb}/^{238}\text{U}$ dates, outside of uncertainty of 5% were removed. Errors are at 2σ .

CA-TIMS U-Pb Geochronology Methods

High-precision U-Pb dates were obtained by chemical abrasion isotope dilution thermal ionization mass spectrometry (CA-TIMS) from analyses of single zircon grains (Table 1), modified after Mattinson (2005). Zircon grains dated by CA-TIMS were selected and plucked from the epoxy mounts based on LA-ICPMS data and CL images, except for the sample with grains that were too small for mounting.

Zircon grains were transferred into 300 μl Teflon PFA microcapsules that were placed in a large-capacity Parr vessel, and the grains were partially dissolved in 120 μl of 29 M HF for 12 hours at 190°C (chemical abrasion; Mattinson, 2005). Grains were returned to 3 ml Teflon PFA beakers, HF was removed, and were immersed in 3.5 M HNO_3 , ultrasonically cleaned for an hour, and fluxed on a hotplate at 80°C for an hour. The HNO_3 was removed, and the grains were rinsed twice in ultrapure H_2O before being reloaded into the 300 μl Teflon PFA microcapsules (rinsed and fluxed in 6 M HCl during sonication and washing of the zircon) and spiked with the EARTHTIME mixed ^{233}U - ^{235}U - ^{205}Pb tracer solution (ET535). Grains were dissolved in Parr vessels in 120 μl of 29 M HF with a trace of 3.5 M HNO_3 at 220°C for 48 hours, dried to fluorides, and re-dissolved in 6 M HCl at 180°C overnight. U and Pb were separated from the zircon matrix using an HCl-based anion-exchange chromatographic procedure (Krogh, 1973), eluted together and dried with 2 μl of 0.05 N H_3PO_4 .

Pb and U were loaded on a single outgassed Re filament in 5 μ l of a silica-gel/phosphoric acid mixture (Gerstenberger and Haase, 1997), and U and Pb isotopic measurements made on a GV Isoprobe-T multicollector thermal ionization mass spectrometer equipped with an ion-counting Daly detector. Pb isotopes were measured by peak-jumping all isotopes on the Daly detector for 160 cycles, and corrected for $0.18 \pm 0.03\%$ /a.m.u. (1σ) mass fractionation. Transitory isobaric interferences due to high-molecular weight organics, particularly on ^{204}Pb and ^{207}Pb , disappeared within approximately 30 cycles, while ionization efficiency averaged 10^4 cps/pg of each Pb isotope. Linearity (to $\geq 1.4 \times 10^6$ cps) and the associated deadtime correction of the Daly detector were determined by analysis of NBS982. Uranium was analyzed as UO_2^+ ions in static Faraday mode on 10^{12} ohm resistors for 300 cycles, and corrected for isobaric interference of $^{233}\text{U}^{18}\text{O}^{16}\text{O}$ on $^{235}\text{U}^{16}\text{O}^{16}\text{O}$ with an $^{18}\text{O}/^{16}\text{O}$ of 0.00206. Ionization efficiency averaged 20 mV/ng of each U isotope. U mass fractionation was corrected using the known $^{233}\text{U}/^{235}\text{U}$ ratio of the ET535 tracer solution.

CA-TIMS U-Pb dates and uncertainties were calculated using the algorithms of Schmitz and Schoene (2007), ET535 tracer solution (Condon et al., 2015) with calibration of $^{235}\text{U}/^{205}\text{Pb} = 100.233$, $^{233}\text{U}/^{235}\text{U} = 0.99506$, and $^{205}\text{Pb}/^{204}\text{Pb} = 11268$, and U decay constants recommended by Jaffey et al. (1971) and $^{238}\text{U}/^{235}\text{U}$ of 137.818 (Hiess et al., 2012). $^{206}\text{Pb}/^{238}\text{U}$ ratios and dates were corrected for initial ^{230}Th disequilibrium using $D_{\text{Th/U}} = 0.2 \pm 0.1$ (2σ) and the algorithms of Crowley et al. (2007), resulting in an increase in the $^{206}\text{Pb}/^{238}\text{U}$ dates of ~ 0.09 Ma. All common Pb in analyses was attributed to laboratory blank and subtracted based on the measured laboratory Pb isotopic composition and associated uncertainty. U blanks are estimated at 0.013 pg.

Weighted mean $^{206}\text{Pb}/^{238}\text{U}$ dates are calculated from equivalent dates (probability of fit >0.05) using Isoplot 3.0 (Ludwig, 2003) with error at the 95% confidence interval.

Error is computed as the internal standard deviation multiplied by the Student's t-distribution multiplier for a two-tailed 95% critical interval and $n-1$ degrees of freedom when the reduced chi-squared statistic, mean squared weighted deviation (MSWD) (Wendt and Carl, 1991), takes a value less than its expectation value plus its standard deviation at the same confidence interval (i.e., $\text{MSWD} < 1 + 2 \cdot \sqrt{2/(n-1)}$).

This error is expanded via multiplication by the $\sqrt{\text{MSWD}}$ when the MSWD is $\geq 1 + 2 \cdot \sqrt{2/(n-1)}$ to accommodate unknown sources of over dispersion. Errors on the weighted mean dates are given as $\pm x / y / z$, where x is the internal error based on analytical uncertainties only, including counting statistics, subtraction of tracer solution, and blank and initial common Pb subtraction, y includes the tracer calibration uncertainty propagated in quadrature, and z includes the ^{238}U decay constant uncertainty propagated in quadrature. Internal errors should be considered when comparing our dates with $^{206}\text{Pb}/^{238}\text{U}$ dates from other laboratories that used the same tracer solution or a tracer solution that was cross-calibrated using EARTHTIME gravimetric standards. Errors including the uncertainty in the tracer calibration should be considered when comparing

our dates with those derived from other geochronological methods using the U-Pb decay scheme (e.g., laser ablation ICPMS). Errors including uncertainties in the tracer calibration and ^{238}U decay constant (Jaffey et al., 1971) should be considered when comparing our dates with those derived from other decay schemes (e.g., $^{40}\text{Ar}/^{39}\text{Ar}$, ^{187}Re - ^{187}Os). Errors on dates from individual analyses are 2σ .

U-Pb Geochronology Results

Thirty grains from ACP yield LA-ICPMS dates of 935 ± 25 to 95 ± 3 Ma. Six grains yield CA-TIMS dates of 99.897 ± 0.073 to 99.544 ± 0.089 Ma. The three youngest dates have a weighted mean date of $99.588 \pm 0.091 / 0.096 / 0.143$ Ma (Mean Squared Weighted Deviation (MSWD) = 1.6, probability of fit = 0.30).

Seventeen grains from AH yield LA-ICPMS dates of 106 ± 6 to 96 ± 3 Ma. Six grains yield CA-TIMS dates of 99.616 ± 0.069 to 99.473 ± 0.085 Ma. The five youngest dates have a weighted mean of $99.514 \pm 0.047 / 0.055 / 0.120$ Ma (MSWD = 1.3, probability of fit = 0.28).

Forty-five grains from COI1-A yield LA-ICPMS dates of 108 ± 4 to 95 ± 2 Ma. Six grains yield CA-TIMS dates of 100.225 ± 0.066 to 99.654 ± 0.065 Ma. The three youngest dates have a weighted mean of $99.670 \pm 0.081 / 0.086 / 0.137$ Ma (MSWD = 0.2, probability of fit = 0.79).

Twenty-nine grains from COI1-B yield LA-ICPMS dates of 1229 ± 25 to 93 ± 2 Ma. Five grains yield CA-TIMS dates of 99.802 ± 0.065 to 99.459 ± 0.066 Ma. The two youngest dates have a weighted mean of $99.497 \pm 0.294 / 0.295 / 0.314$ Ma (MSWD = 2.7, probability of fit = 0.10).

Six grains from COI-2 yield CA-TIMS dates of 99.597 ± 0.064 to 99.208 ± 0.089 Ma. The three youngest dates have a weighted mean of $99.264 \pm 0.089 / 0.094 / 0.142$ Ma (MSWD = 1.4, probability of fit = 0.25).

Eleven grains from DE1 yield LA-ICPMS dates of 173 ± 6 to 94 ± 3 Ma.

Twenty-one grains from DE2 yield LA-ICPMS dates of 108 ± 4 to 94 ± 2 Ma. Five grains yield CA-TIMS dates of 100.975 ± 0.075 to 99.505 ± 0.066 Ma. The four youngest dates have a weighted mean of $99.567 \pm 0.056 / 0.063 / 0.124$ Ma (MSWD = 2.5, probability of fit = 0.06).

Fifteen grains from DE3 yield LA-ICPMS dates of 110 ± 3 to 92 ± 2 Ma. Six grains yield CA-TIMS dates of 99.449 ± 0.068 to 99.339 ± 0.065 Ma that have a weighted mean of $99.368 \pm 0.035 / 0.046 / 0.116$ Ma (MSWD = 1.5, probability of fit = 0.17).

Twenty-seven grains from E1 yield LA-ICPMS dates of 110 ± 7 to 96 ± 4 Ma. Eight grains yield CA-TIMS dates of 101.033 ± 0.066 to 99.394 ± 0.076 Ma. The five youngest dates have a weighted mean of $99.451 \pm 0.042 / 0.052 / 0.118$ Ma (MSWD = 2.0, probability of fit = 0.09).

Forty grains from JETA yield LA-ICPMS dates of 1010 ± 28 to 93 ± 2 Ma. Eight grains yield CA-TIMS dates of 99.302 ± 0.080 to 98.920 ± 0.064 Ma. The four youngest dates have a weighted mean of $98.931 \pm 0.054 / 0.062 / 0.123$ Ma (MSWD = 0.1, probability of fit = 0.93).

Forty-five grains from RHA yield LA-ICPMS dates of 108 ± 3 to 94 ± 4 Ma. Six grains yield CA-TIMS dates of 99.690 ± 0.065 to 99.517 ± 0.079 Ma. The four youngest dates have a weighted mean of $99.577 \pm 0.054 / 0.062 / 0.123$ Ma (MSWD = 1.6, probability of fit = 0.20).

Forty-seven grains from RHB yield LA-ICPMS dates of 1751 ± 39 to 92 ± 6 Ma. Six grains yield CA-TIMS dates of 99.829 ± 0.072 to 99.540 ± 0.065 Ma.

Forty-eight grains from WS10 yield LA-ICPMS dates of 1882 ± 46 to 93 ± 3 Ma. Six grains yield CA-TIMS dates of 100.084 ± 0.065 to 99.639 ± 0.065 Ma. The two youngest dates have a weighted mean of $99.771 \pm 0.291 / 0.293 / 0.312$ Ma (MSWD = 0.6, probability of fit = 0.42).

References

- Condon D.J., Schoene B., McLean N.M., Bowring S.A., Parrish R, 2015, Metrology and traceability of U-Pb isotope dilution geochronology (EARTHTIME Tracer Calibration Part I): *Geochimica et Cosmochimica Acta* 164: 464-480.
- Crowley, J.L., Schoene, B., Bowring, S.A., 2007, U-Pb dating of zircon in the Bishop Tuff at the millennial scale: *Geology* 35: 1123-1126.
- Gerstenberger, H., Haase, G., 1997, A highly effective emitter substance for mass spectrometric Pb isotope ratio determinations: *Chemical Geology* 136: 309-312.
- Hiess, J., Condon, D.J., McLean, N., Noble, S. R., 2012, $^{238}\text{U}/^{235}\text{U}$ systematics in terrestrial uranium-bearing minerals: *Science* 335: 1610-1614.
- Jaffey, A.H., Flynn, K.F., Glendenin, L.E., Bentley, W.C., Essling, A.M., 1971, Precision measurements of half-lives and specific activities of ^{235}U and ^{238}U : *Physical Review C*, 4: 1889-1906.
- Krogh, T.E., 1973, A low contamination method for hydrothermal decomposition of zircon and extraction of U and Pb for isotopic age determination: *Geochimica et Cosmochimica Acta* 37: 485-494.
- Kuiper, Y.D., Murray, D.P., Ellison, S., Crowley, J.L. 2022. U-Pb detrital zircon analysis of sedimentary rocks of the southeastern New England Avalon terrane in the U.S. Appalachians:

Evidence for a separate crustal block. New Developments in the Appalachian-Caledonian-Variscan Orogen. Geological Society of America. DOI: <https://doi.org/10.1130/SPE554>

Ludwig, K.R., 2003, User's Manual for Isoplot 3.00. Berkeley Geochronology Center: Berkeley, CA, 70 p.

Mattinson, J.M., 2005, Zircon U-Pb chemical abrasion ("CA-TIMS") method: combined annealing and multi-step partial dissolution analysis for improved precision and accuracy of zircon ages: *Chemical Geology* 220:47-66.

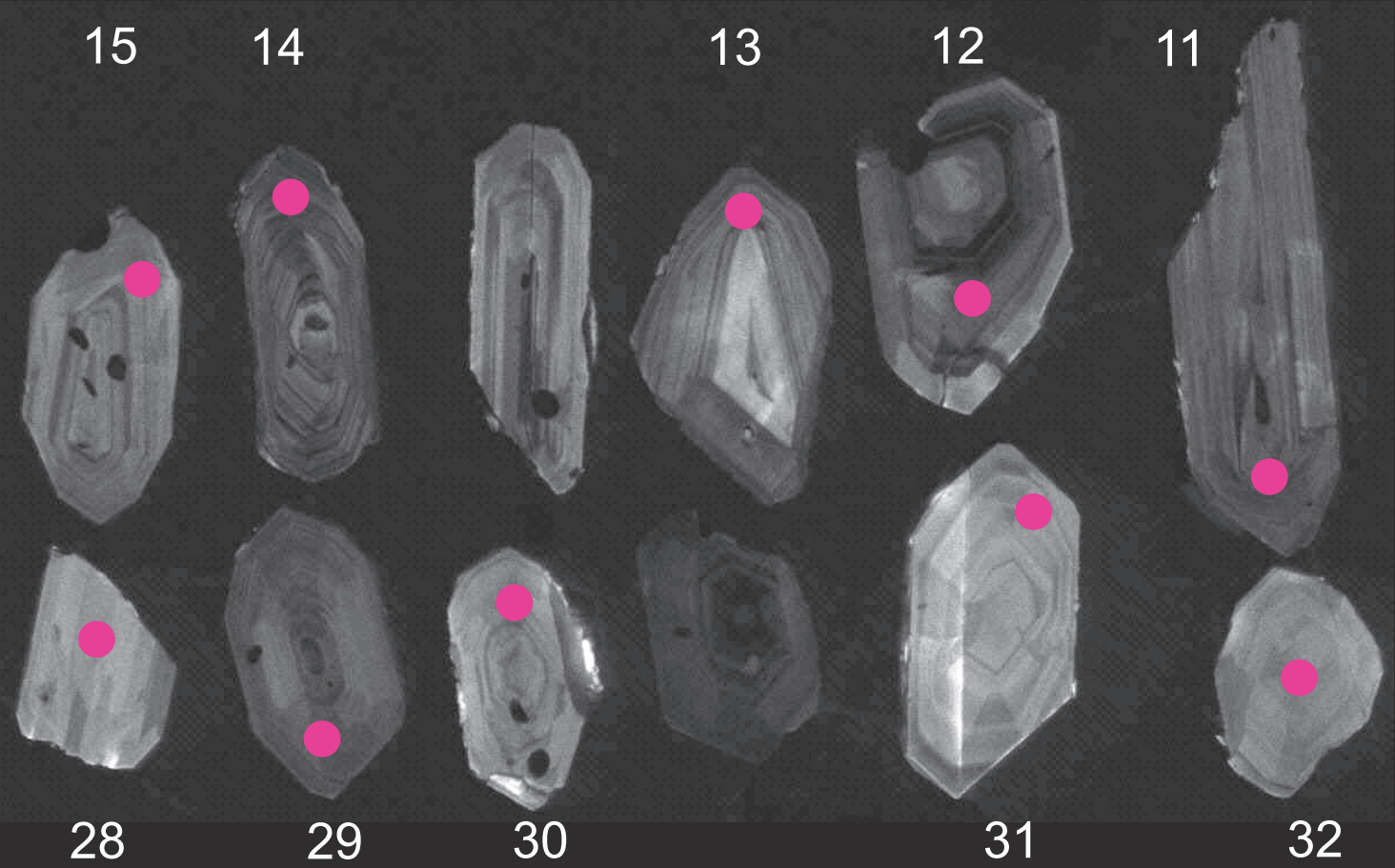
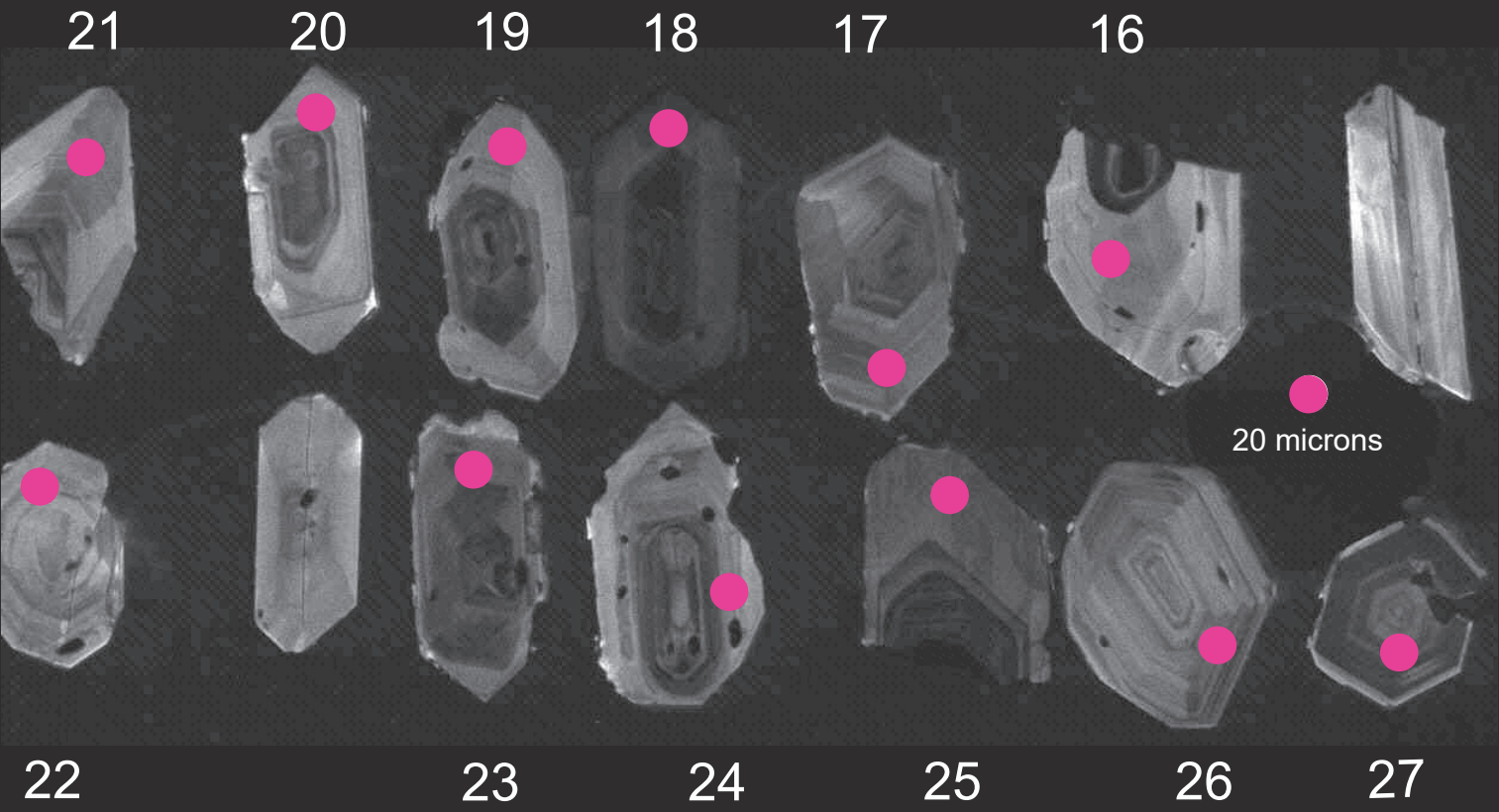
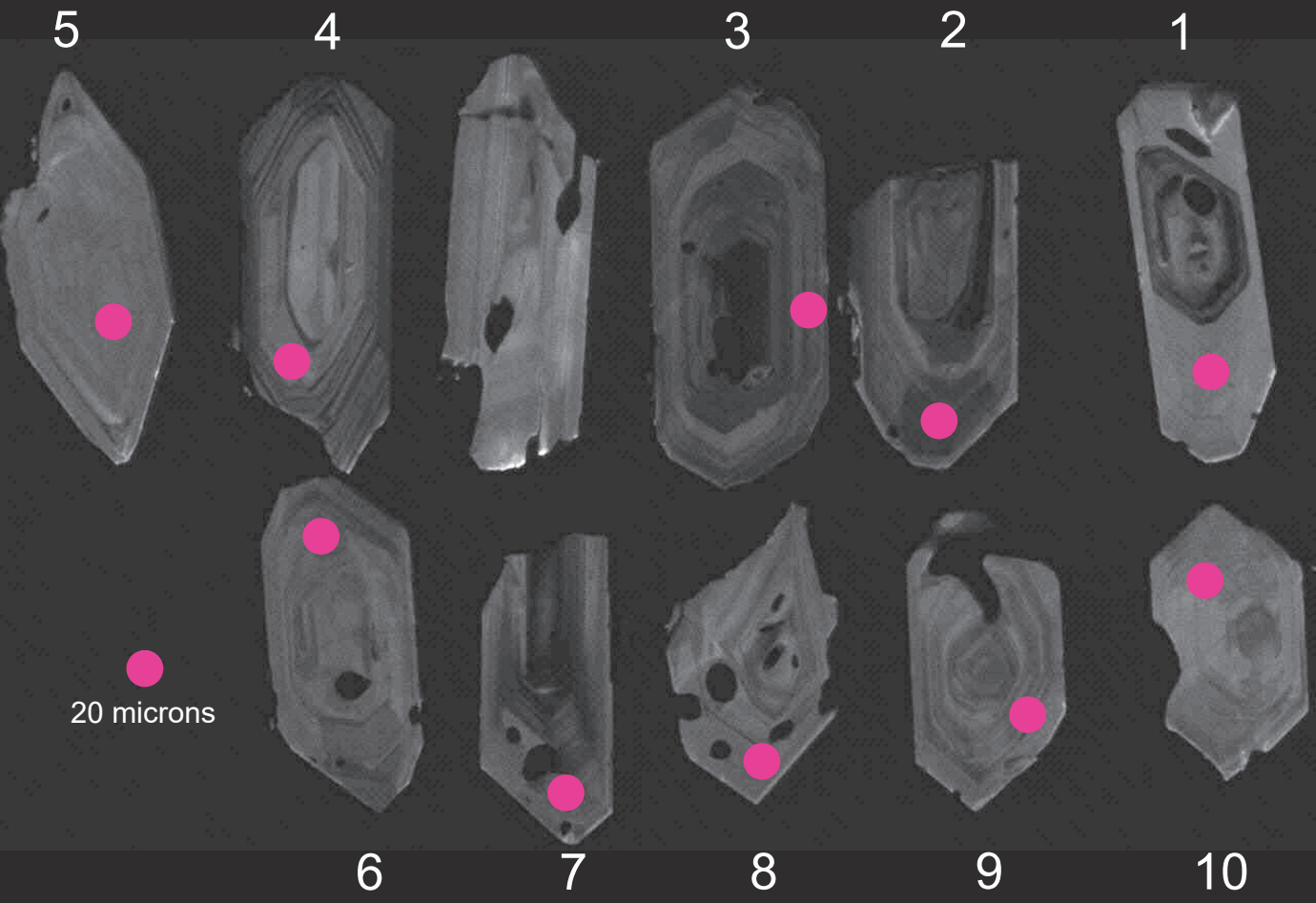
Schmitz, M.D., Schoene, B., 2007, Derivation of isotope ratios, errors and error correlations for U-Pb geochronology using ^{205}Pb - ^{235}U -(^{233}U)-spiked isotope dilution thermal ionization mass spectrometric data: *Geochemistry, Geophysics, Geosystems* (G^3) 8, Q08006, doi:10.1029/2006GC001492.

Sláma, J., Košler, J., Condon, D.J., Crowley, J.L., Gerdes, A., Hanchar, J.M., Horstwood, M.S.A., Morris, G.A., Nasdala, L., Norberg, N., Schaltegger, U., Schoene, B., Tubrett, M.N., Whitehouse, M.J., 2008, Plešovice zircon — A new natural reference material for U–Pb and Hf isotopic microanalysis. *Chemical Geology*, 249: 1-35.

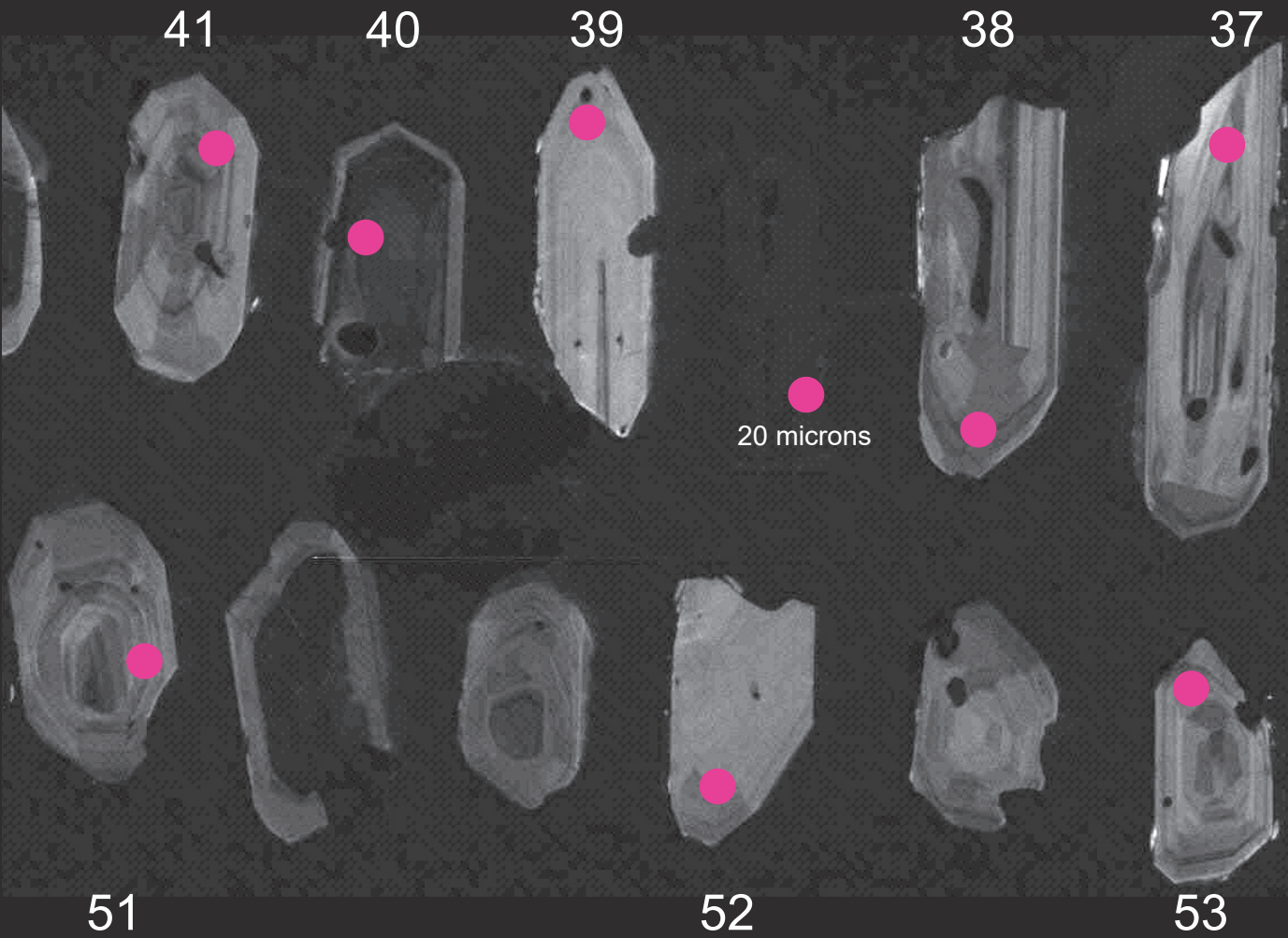
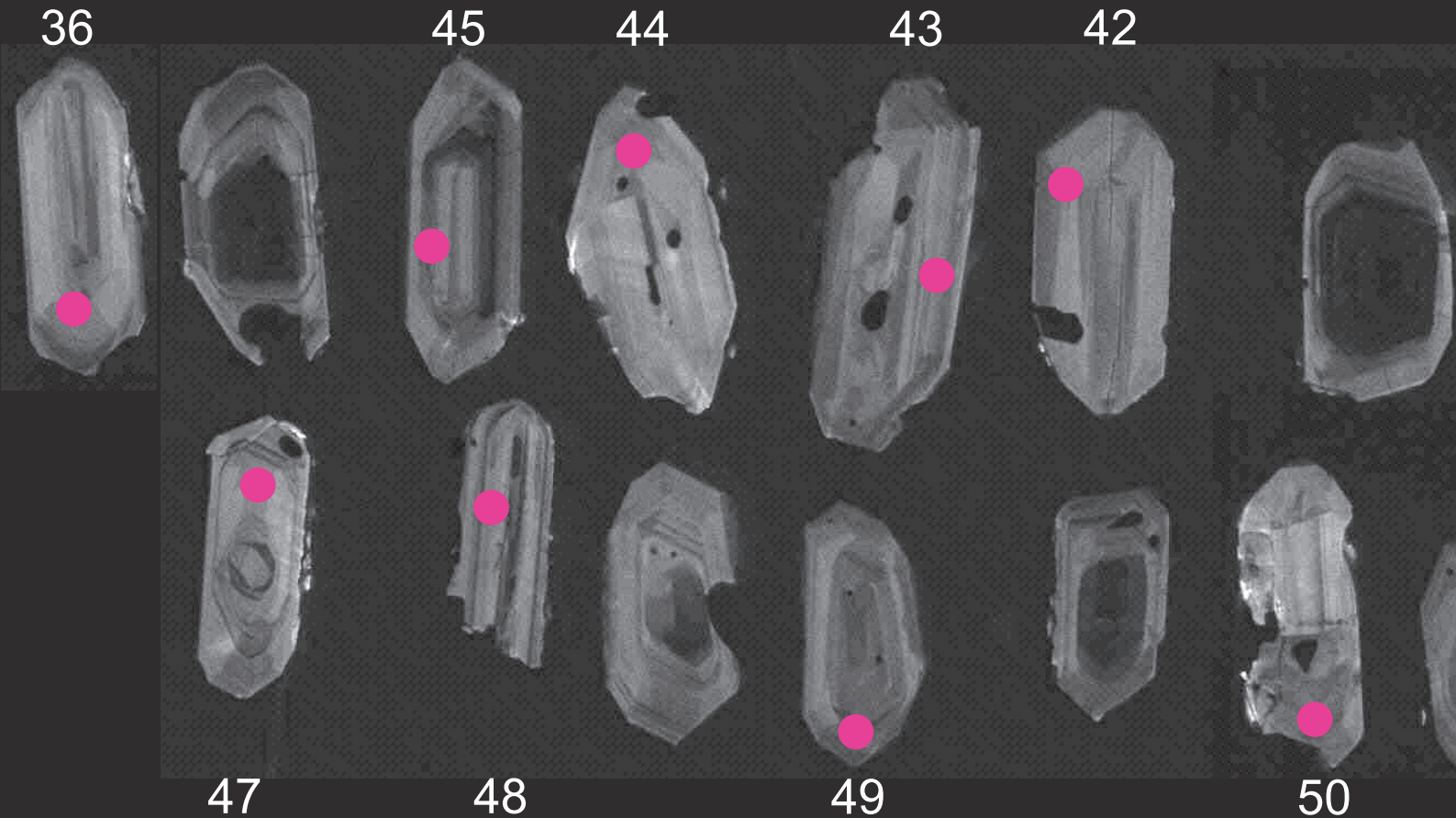
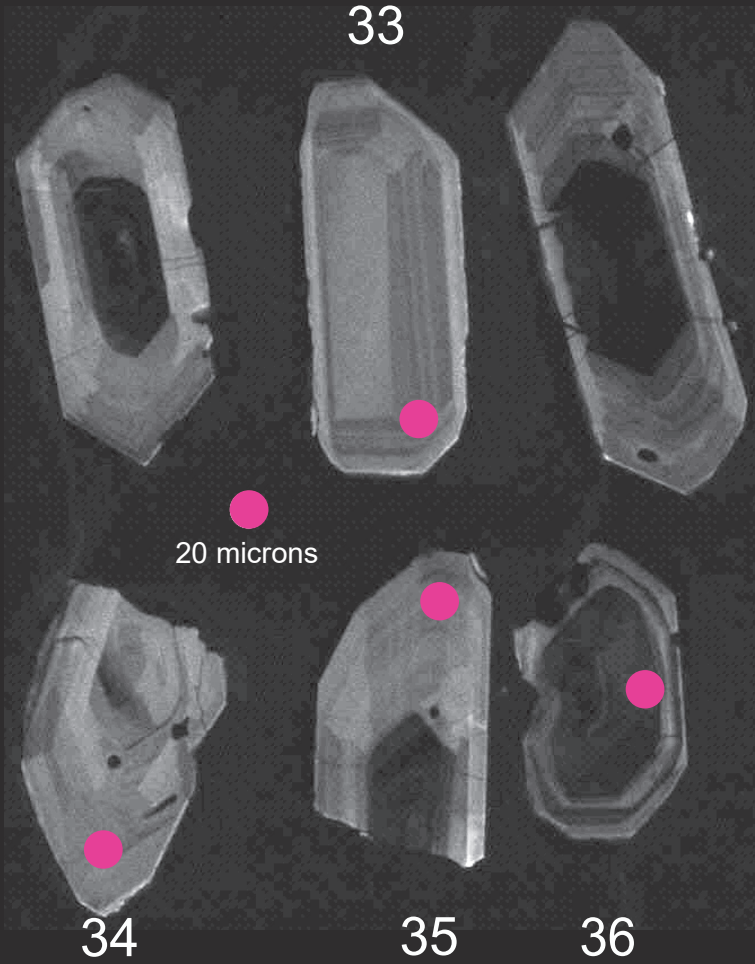
Watson, E.B., Wark, D.A., Thomas, J.B., 2006, Crystallization thermometers for zircon and rutile. *Contributions to Mineralogy and Petrology*, 151: 413-433.

Wiedenbeck, M., Alle, P., Corfu, F., Griffin, W. , Meier, M., Oberli, F., Quadt, A.V., Roddick, J., Spiegel, W. 1995, Three natural zircon standards for U-Th-Pb, Lu-Hf, trace element and REE Analyses. *Geostandards Newsletter*, 19: 1-23.

Analytical Sample: ACP
Field Sample: Ash Croc Pete
Mussentuchit Ash Zone 1 (MAZ 1)



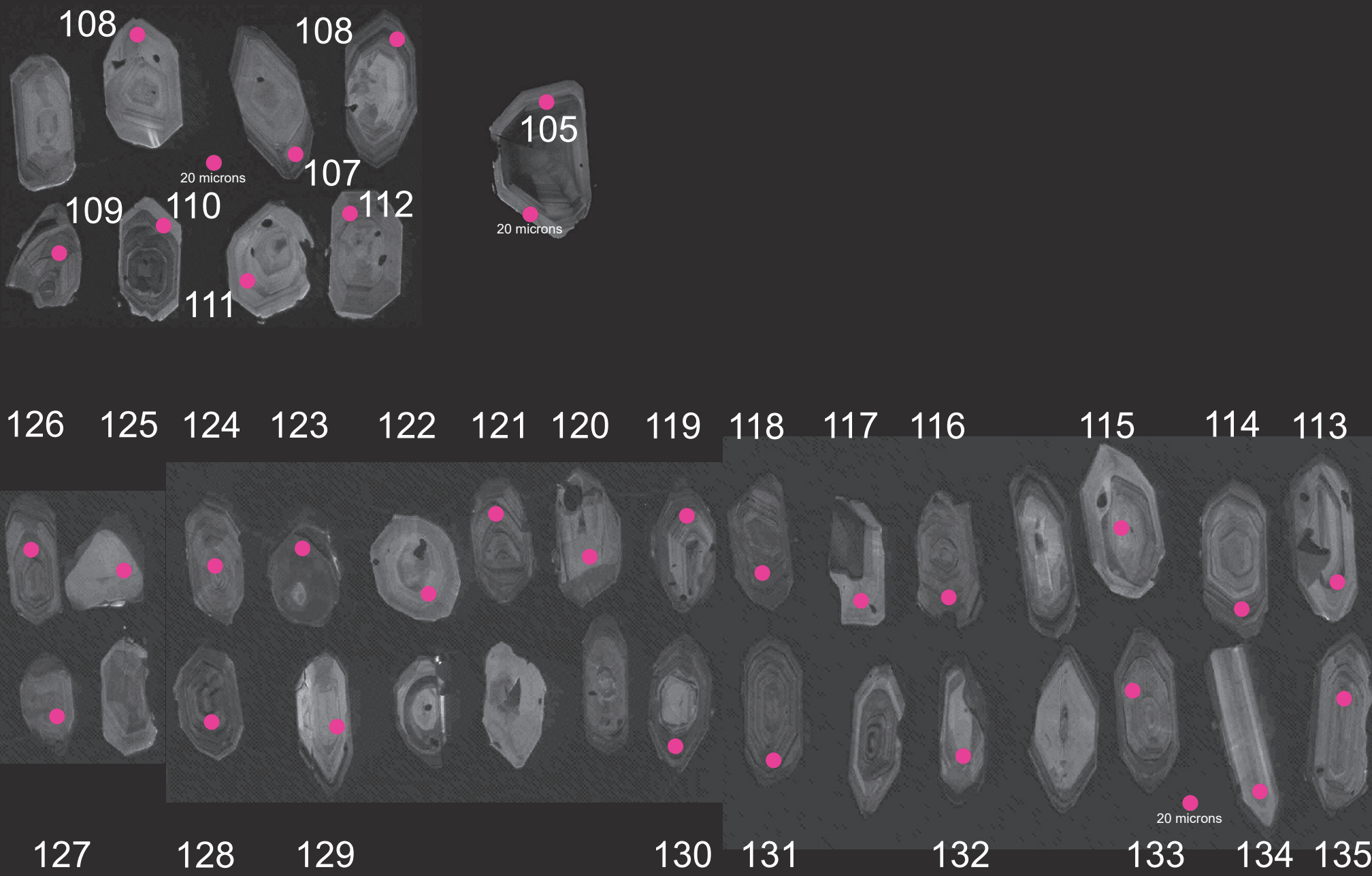
Analytical Sample: AH
Field Sample: ASH HOLE
Mussentuchit Ash Zone 2 (MAZ 2)



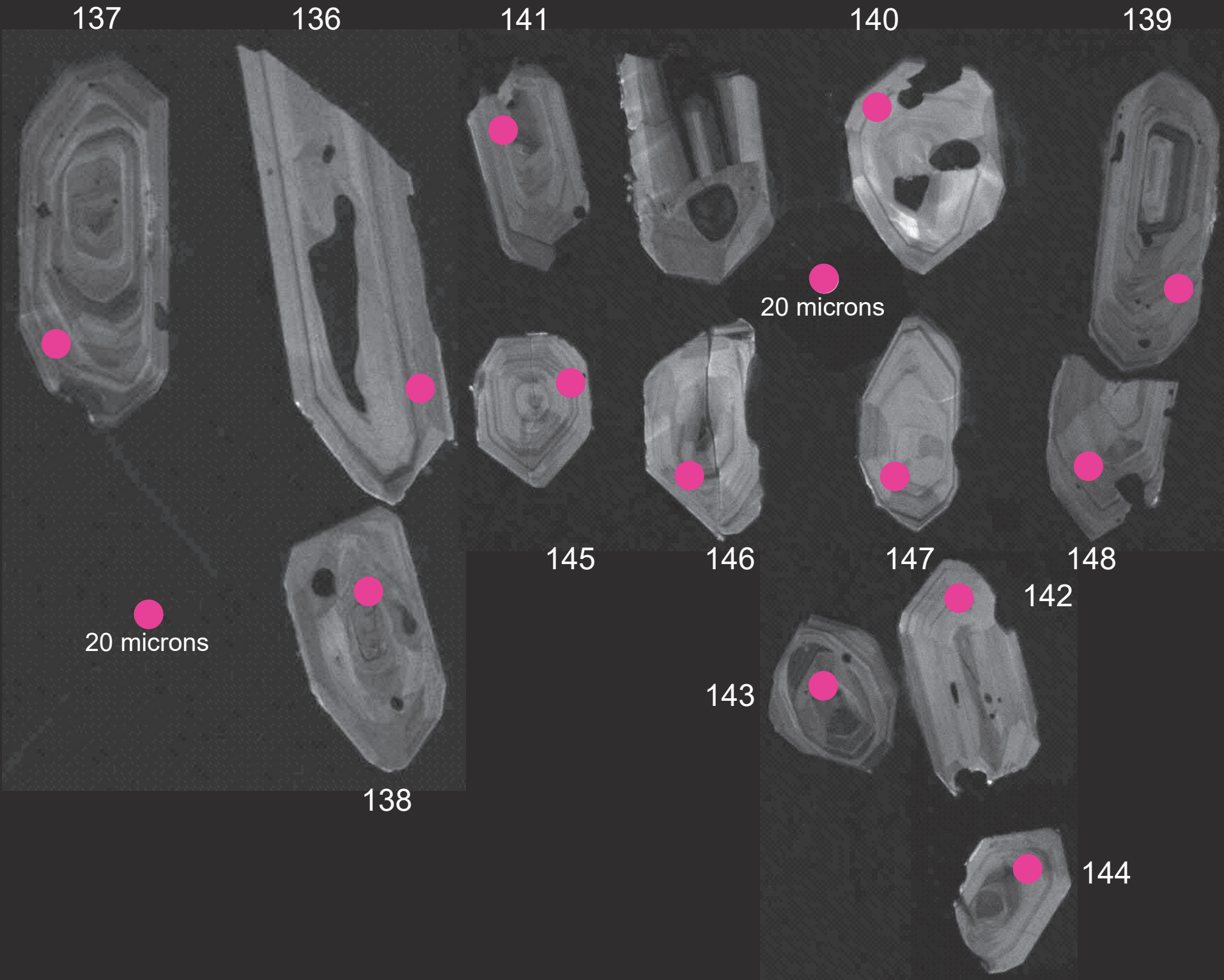
Analytical Sample: COI-1A
Field Sample: Cliffs of Insanity-1A
Mussentuchit Ash Zone 1 (MAZ 1)

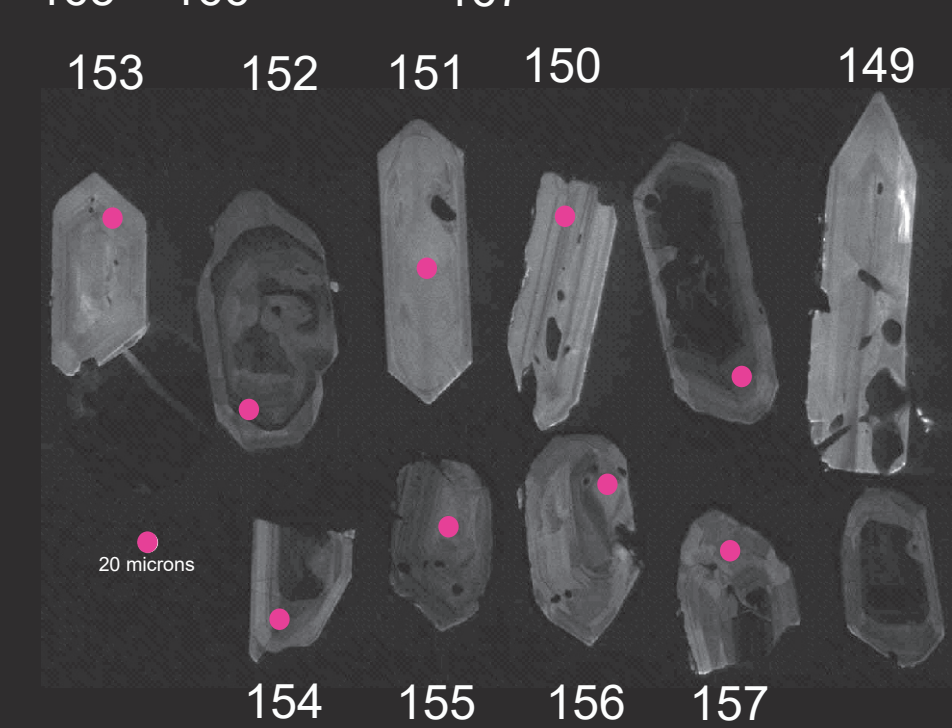
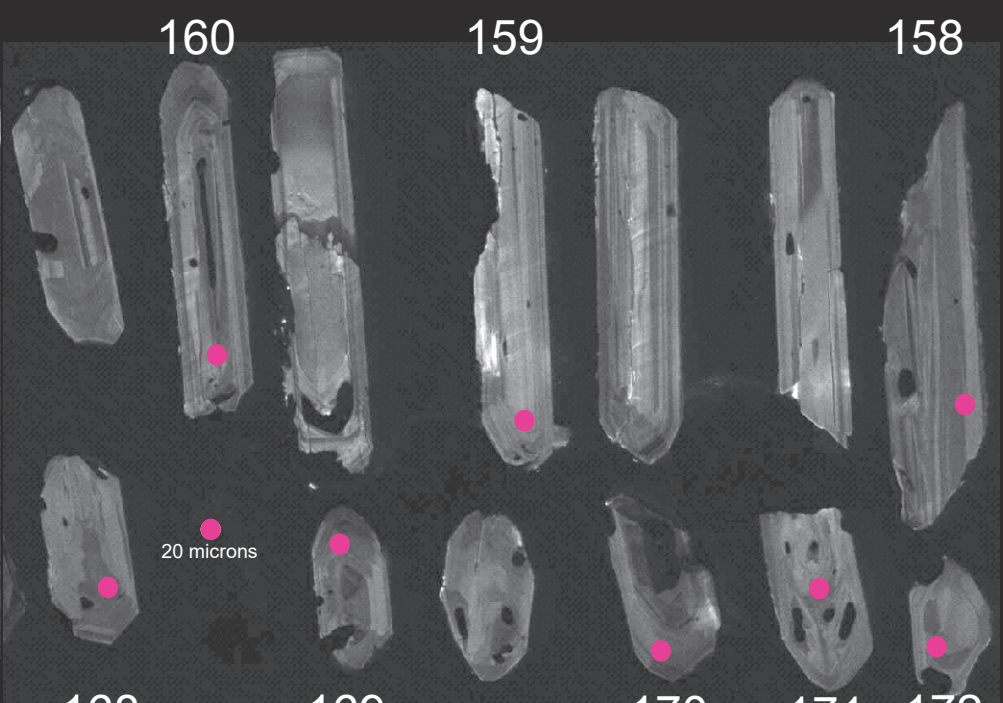
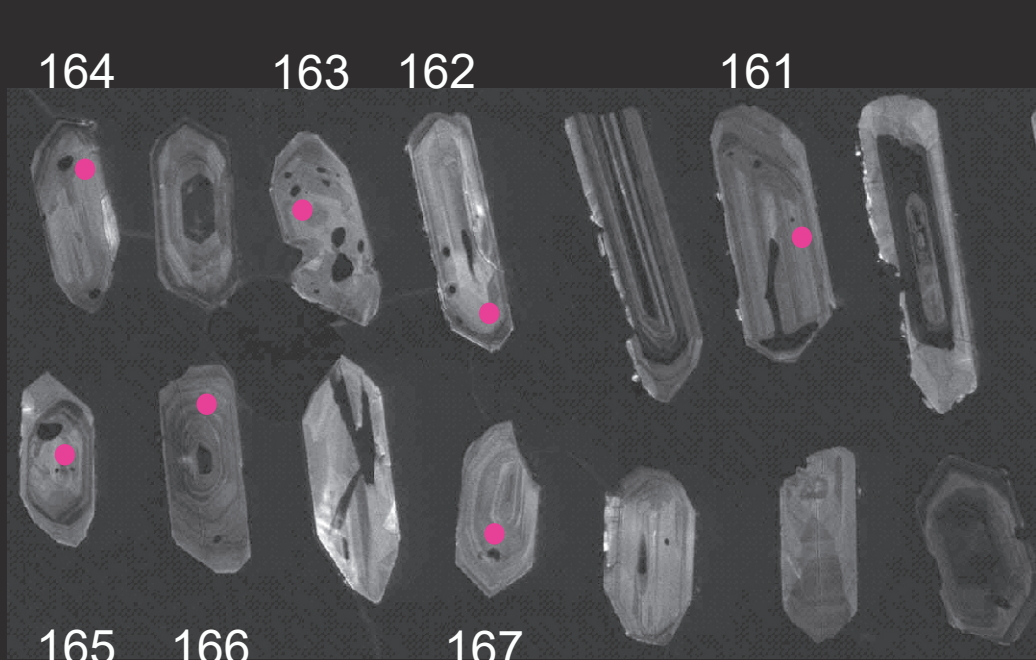


Analytical Sample: COI-1B
Field Sample: Cliffs of Insanity-1B
Mussentuchit Ash Zone 1 (MAZ 1)



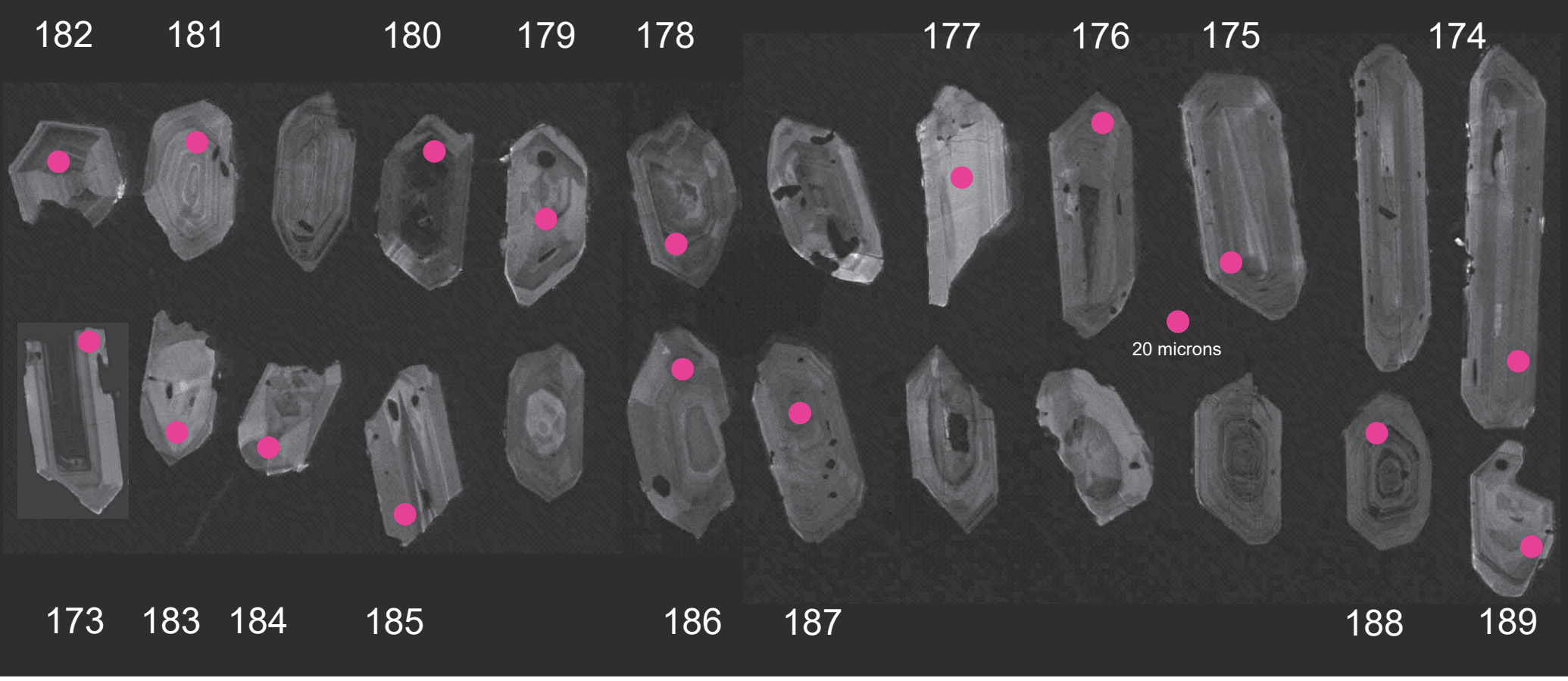
Analytical Sample: DE1
Field Sample: Deep Eddy 1
Mussentuchit Ash Zone 1 (MAZ 1)

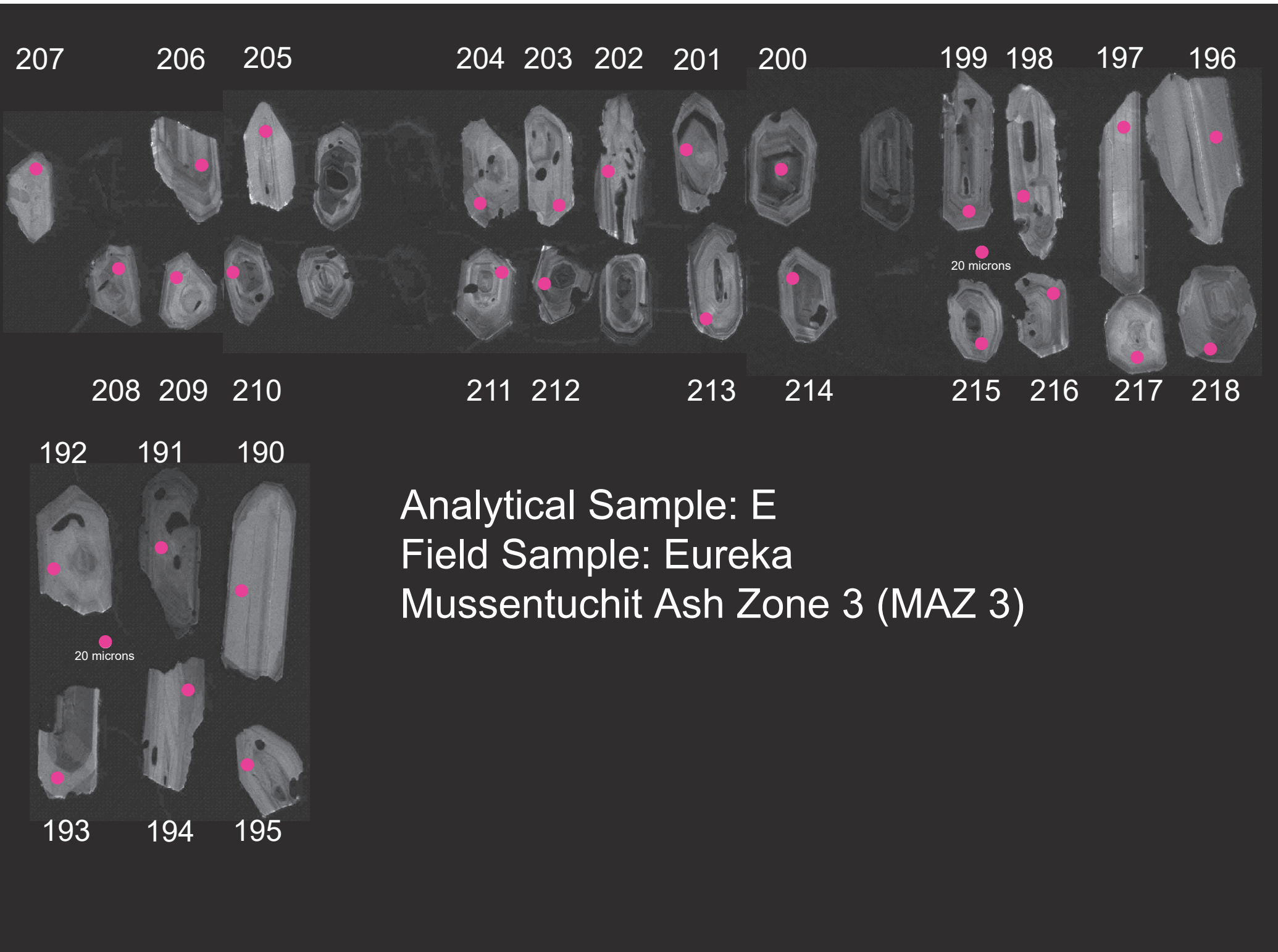




Analytical Sample: DE2
Field Sample: Deep Eddy 2
Mussentuchit Ash Zone 2 (MAZ 2)

Analytical Sample: DE3
Field Sample: Deep Eddy 3
Mussentuchit Ash Zone 3 (MAZ 3)

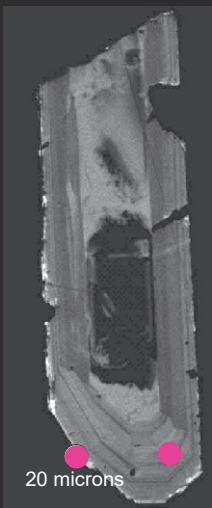
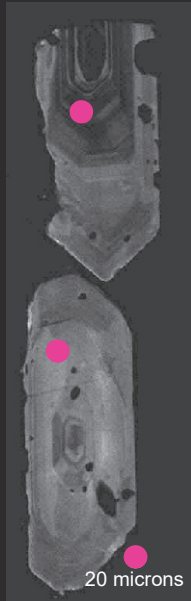




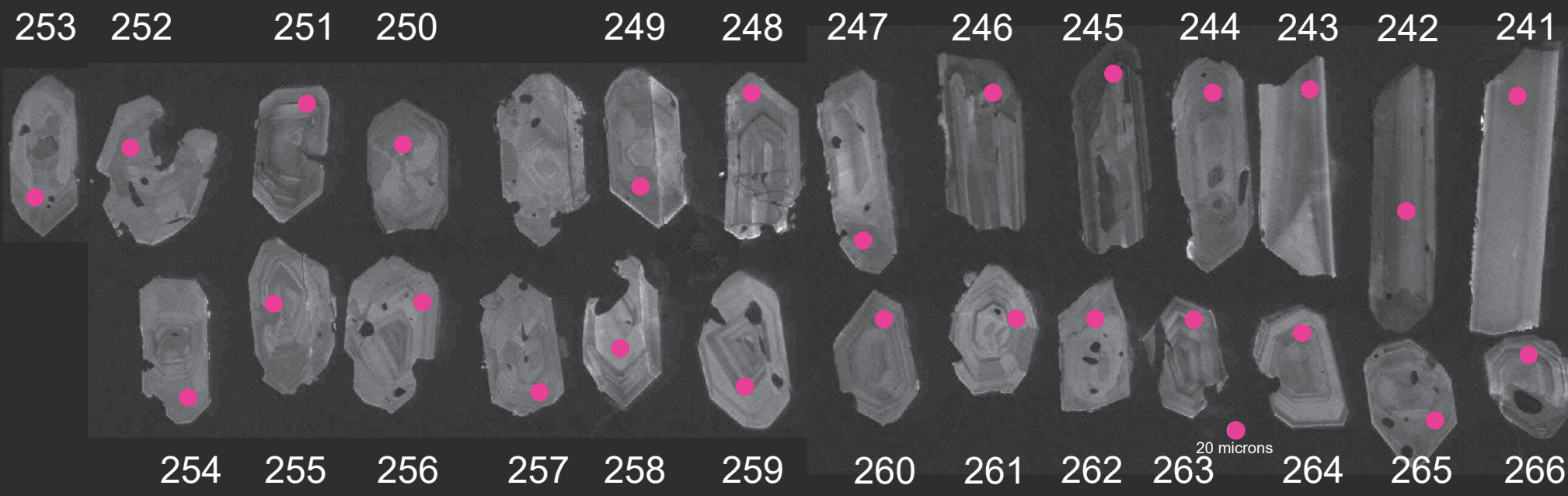
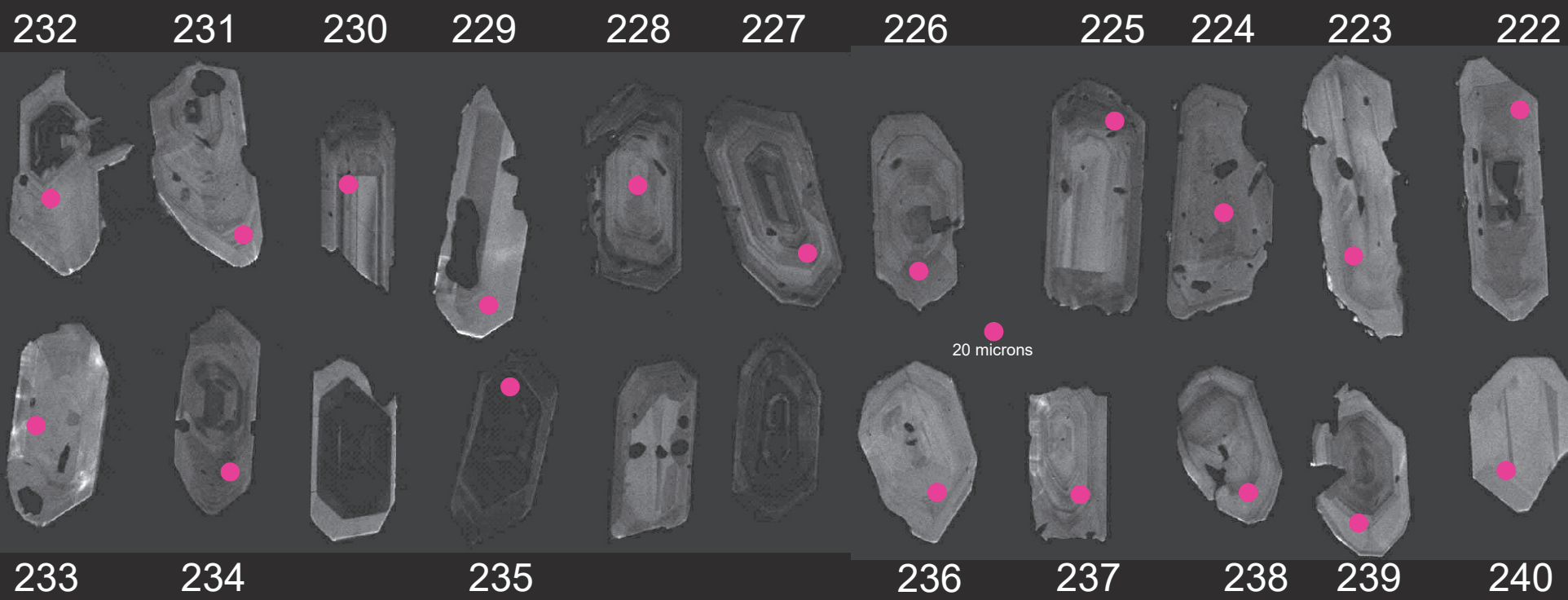
Analytical Sample: JETA
Field Sample: JET_A (James Edmund Tucker)
Mussentuchit Ash Zone 4 (MAZ 4)

220

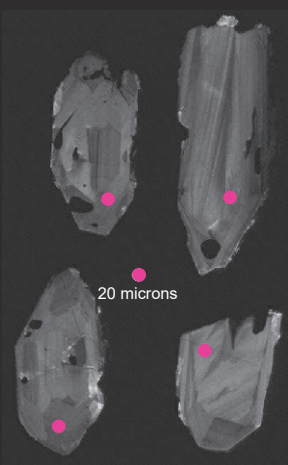
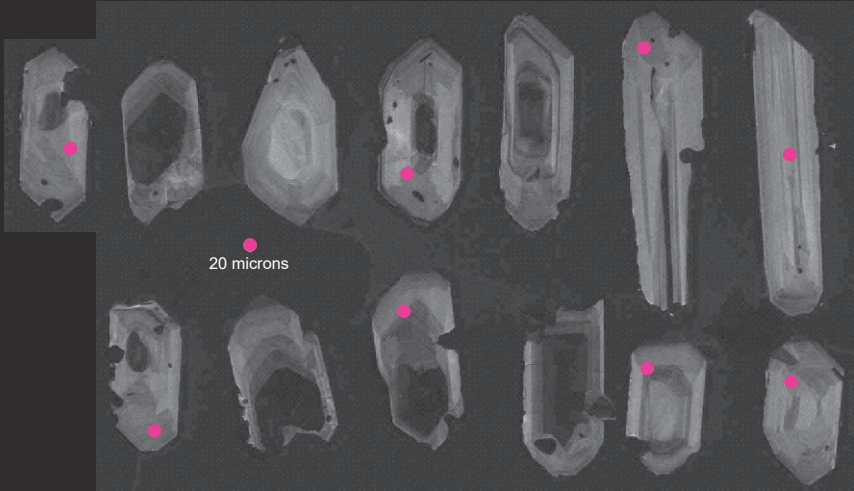
219



221



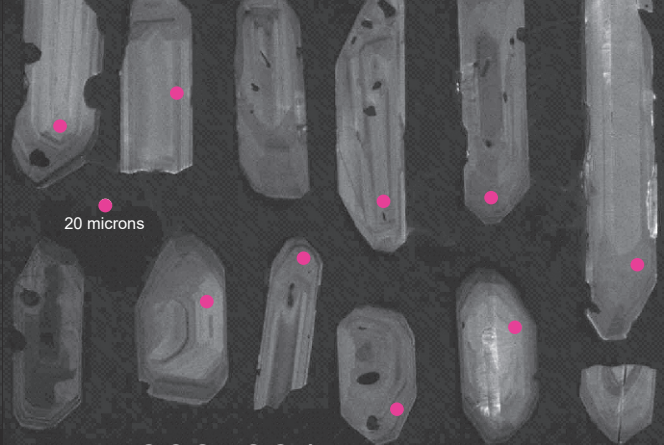
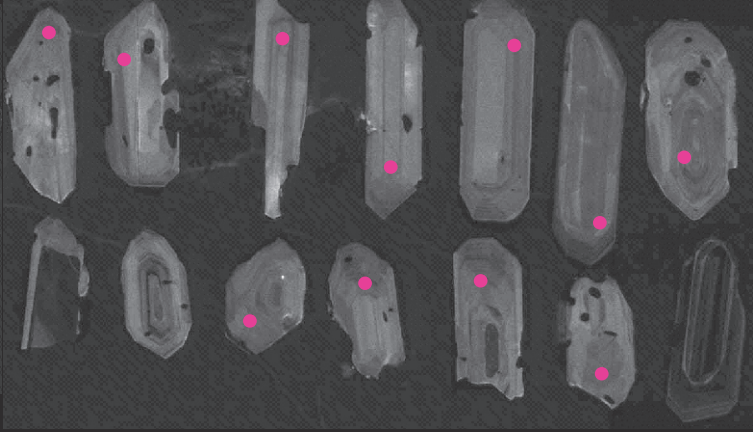
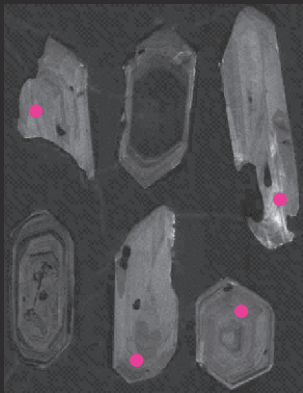
275 274 273 272 268 267



Analytical Sample: RHA
Field Sample: Red
Herring-A
Mussentuchit Ash
Zone 1 (MAZ 1)

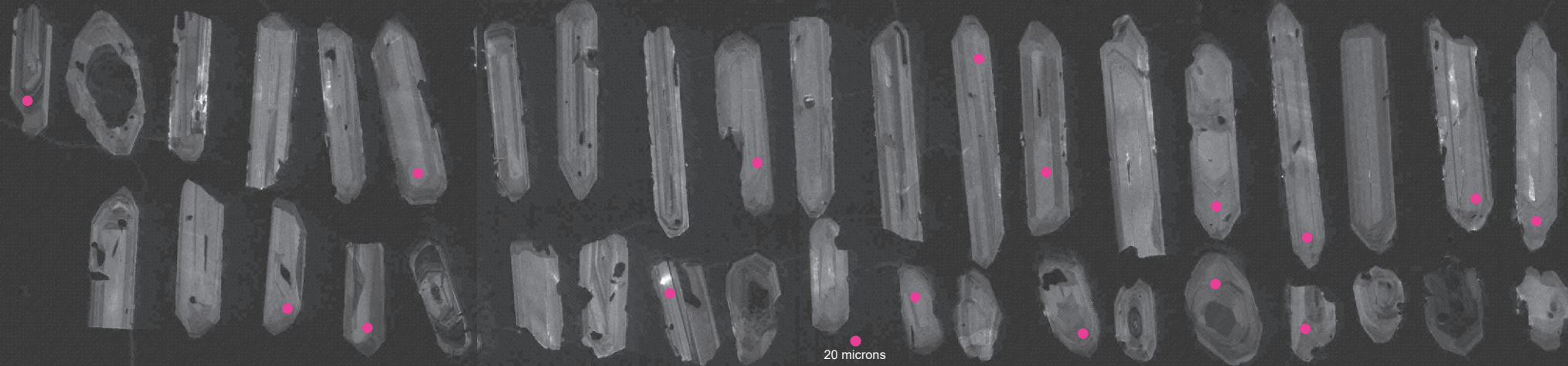
276 277 278 279 269 270

293 292 291 290 289 288 287 286 285 284 283 282 281 280



294 295 296 297 298 299 300 301 302 303

312 311 310 309 308 307 306 305 304



313 314 315 316 317 318 319

Analytical Sample: WS10
Field Sample: WS10-V695
Mussentuchit Ash Zone 2 (MAZ 2)

